

Qi He and Wentao Hu these authors are contributed equally to this work.

### Key Points:

- Tadpole-shaped Fe-Ni-S-Ti nanoparticles have been found in the impact melt glass spherule of an agglutinate in Chang'e-5 lunar soil
- The nanoparticles made up of Fe-Ni-S heads and with tails made up of Fe-Ti-O (ilmenite)
- The nanoparticles provide a new example of viscous fingering and ilmenite dendrites point to high-T chemical gardens in lunar impact melt

### Supporting Information:

Supporting Information may be found in the online version of this article.

### Correspondence to:

L. Xiao,  
[longxiao@cug.edu.cn](mailto:longxiao@cug.edu.cn)

### Citation:

He, Q., Hu, W., Xiao, L., Zhang, X., Wang, Z., Qian, Y., et al. (2024). Tadpole-shaped nanoparticles in impact melt and implication of high temperature chemical garden in lunar soil. *Journal of Geophysical Research: Planets*, 129, e2024JE008584. <https://doi.org/10.1029/2024JE008584>

Received 19 JUL 2024

Accepted 25 OCT 2024

### Author Contributions:

**Conceptualization:** Qi He, Wentao Hu, Long Xiao

**Data curation:** Qi He, Wentao Hu, Xiang Zhang, Yiheng Li

**Formal analysis:** Yuqing Chang, Zhiyong Xiao, Xiang Wu

**Funding acquisition:** Zaicong Wang






**Investigation:** Long Xiao, Xiang Zhang, Yuqi Qian, Jinfu Shu, Jiawei Zhao, Yuqing Chang, Chen Li, Zhiyong Xiao, Xiaoping Zhang, Yiheng Li, Siyuan Zhao, Jun Huang, Jiannan Zhao, Jiang Wang, Yang Li

**Methodology:** Qi He, Wentao Hu, Xiang Zhang, Yuqi Qian, Jinfu Shu, Jiawei Zhao, Yuqing Chang, Yiheng Li, Jiannan Zhao, Jiang Wang, Zhaochu Hu, Keqing Zong, Zhenbing She

**Project administration:** Long Xiao

© 2024. American Geophysical Union. All Rights Reserved.

# Tadpole-Shaped Nanoparticles in Impact Melt and Implication of High Temperature Chemical Garden in Lunar Soil

Qi He<sup>1</sup> , Wentao Hu<sup>2</sup>, Long Xiao<sup>1,3</sup> , Xiang Zhang<sup>2</sup>, Zaicong Wang<sup>1</sup> , Yuqi Qian<sup>4</sup> , Jinfu Shu<sup>5</sup>, Jiawei Zhao<sup>1</sup>, Yuqing Chang<sup>2</sup>, Chen Li<sup>6</sup>, Zhiyong Xiao<sup>7</sup> , Xiaoping Zhang<sup>3</sup> , Yiheng Li<sup>1</sup>, Papineau Dominic<sup>8,9</sup>, Siyuan Zhao<sup>1</sup>, Jun Huang<sup>1</sup> , Jiannan Zhao<sup>1</sup> , Jiang Wang<sup>1</sup>, Xiang Wu<sup>1</sup> , Zhaochu Hu<sup>1</sup>, Keqing Zong<sup>1</sup>, Zhenbing She<sup>8</sup>, and Yang Li<sup>6</sup> 

<sup>1</sup>State Key Laboratory of Geological Processes and Mineral Resources, Planetary Science Institute, School of Earth Sciences, China University of Geosciences, Wuhan, China, <sup>2</sup>State Key Laboratory of Metastable Materials Science and Technology, Center for High Pressure Science, Yanshan University, Qinhuangdao, China, <sup>3</sup>State Key Laboratory of Lunar and Planetary Sciences, Macau University of Science and Technology, Macau, China, <sup>4</sup>Department of Earth Sciences, The University of Hong Kong, Hong Kong, China, <sup>5</sup>Center for High Pressure Science and Technology Advanced Research, Shanghai, China, <sup>6</sup>Center for Lunar and Planetary Sciences, Institute of Geochemistry, Chinese Academy of Sciences, Guiyang, China, <sup>7</sup>Planetary Environmental and Astrobiological Research Laboratory, School of Atmospheric Sciences, Sun Yat-sen University, Zhuhai, China, <sup>8</sup>State Key Laboratory of Biogeology and Environmental Geology, School of Earth Sciences, China University of Geosciences, Wuhan, China, <sup>9</sup>Institute of Deep Sea Science and Engineering, Chinese Academy of Sciences, Sanya, China

**Abstract** Nanoparticles within lunar soil grains are a primary product of space weathering. The microstructural and chemical characteristics of the nanoparticles are diverse and their formation mechanisms are still under debate. In this paper, for the first time, tadpole-shaped nanoparticles (with Fe-Ni(-S) head and Fe-Ti-O tail) were found in the impact melt glass spherule of an agglutinate in the returned Chang'e-5 lunar soil, and their possible formation mechanisms were discussed. In terms of the Fe-Ni(-S) “head” formation mechanisms, they probably produced by shock-induced dissemination. Another possibility is that the Fe-Ni(-S) heads were derived from the impact glass due to liquid immiscibility. The S degassing of FeS was contributed to nanophase Fe-Ni metal. For the Fe-Ti-O tails, they are devitrified ilmenites, nucleated as a result of the passage of the Fe nanoparticles through the melt. These nanoparticles formed though impact-induced nonequilibrium growth and recorded the movement and migration of the Fe-Ni-S nanoparticles within the melt. The tadpole-shape nanoparticles provide a new example of viscous fingering in impact melts and the associated ilmenite dendrites point to the formation of high-temperature chemical gardens in lunar impact melt.

**Plain Language Summary** The Moon's surface is a hostile environment. Micrometeorite impacts and solar wind irradiation have modified lunar surface for billions of years, producing large amount of nanoscale metal particles within lunar soil grains. These nanoparticles show a variety of microstructure and chemical characteristics, and the formation mechanisms are still controversial. From the returned Chang'e-5 lunar soil, we first discovered tadpole-shaped Fe-Ni-S-Ti nanoparticles in the impact melt glass of an agglutinate particle. The composition of the nanoparticles “metal heads” indicates they could derive from impact-induced dissemination in melts or unmixing of two immiscible melts between Fe-S melt and silicate melt. S outgassing from FeS led to the creation of nanoscale Fe-Ni metallic particles. The Fe-Ti-O tails of the nanoparticles indicate that these particles are most likely exsolution from melt during the movement and migration of the Fe-Ni-S nanoparticles. Our observations provide a viscous fingering in impact melts of nano-phase metal particles in lunar soil. The presence of ilmenite dendrites suggests the occurrence of high-temperature chemical gardens (self-organizing nonequilibrium process) during the impact process.

## 1. Introduction

Micrometeorite impacts, solar wind and cosmic ray irradiation are the main drivers of space weathering for airless bodies (Hapke, 2001; Pieters et al., 2000; Pieters & Noble, 2016). Lunar returned samples (e.g., Apollo and Luna samples) exhibit well-preserved evidence of space weathering, in which numerous nano-scale metals were discovered in the surface regolith (Heiken, 1975; Li, Guo, et al., 2022; Pieters & Noble, 2016; Thompson

**Resources:** Zaicong Wang, Xiang Wu, Zhaochu Hu, Keqing Zong, Zhenbing She  
**Supervision:** Long Xiao, Yang Li  
**Validation:** Xiaoping Zhang  
**Visualization:** Jun Huang  
**Writing – original draft:** Qi He, Wentao Hu, Long Xiao, Xiang Zhang, Zaicong Wang, Yuqi Qian, Jiawei Zhao, Yuqing Chang, Chen Li, Xiaoping Zhang, Yiheng Li, Siyuan Zhao, Jiannan Zhao, Xiang Wu

et al., 2021). Previous studies on lunar returned samples showed that the regolith grains contain many spherical nano-scale particles, named nanoparticles (np), including pure Fe (called as npFe<sup>0</sup> here after) and multiphase npFe-Ni, iron-sulfides, iron-silicides, iron-oxides (be collectively called as np-metal here after), and silicon-oxide (Gopon et al., 2017; Gu et al., 2018; Keller & McKay, 1997; Matsumoto et al., 2021; Pieters & Noble, 2016). The grain size of the nanoparticles varies significantly: nanoparticles within the depositional rim of mafic minerals have diameters of ~1–10 nm; and large micron-sized particles (~40 nm – 2 μm) have been discovered mostly within impact melts (agglutinates and spherical glass beads (Britt & Pieters, 1994; Pieters & Noble, 2016). The production of these nanoparticles in lunar soil grains has changed both the chemical and optical properties of lunar regolith, thus their formation are pivotal to lunar surface evolution (Hapke, 2001; Lucey & Noble, 2008; Noble et al., 2007; Pieters & Noble, 2016; Taylor et al., 2001).

There are several proposed formation mechanisms for these nanoparticles, including various processes associated with meteorite impacts and solar wind irradiation (Basu, 2005; Hapke, 2001; Noguchi et al., 2011). The npFe<sup>0</sup> in the depositional rims of minerals and in agglutinate glasses may be the products of meteorite vaporization and deposition (Keller & McKay, 1993, 1997). The highly enriched heavy iron isotope ( $\delta^{56}\text{Fe}$ ) signature in npFe<sup>0</sup> confirms that they likely originated from the depositional process generated by solar wind particle sputtering or micrometeorite impacts (Wang et al., 2012). Part of the npFe<sup>0</sup> in the amorphous rim may be produced by the reduction of Fe<sup>2+</sup> from Fe-bearing minerals by solar wind hydrogen (Housley et al., 1973) or by fayalitic olivine decomposition (Z. Guo, Li, Li, Wen, Tai, et al., 2022), which is supported by simulated pulsed-laser irradiation experiments on iron-bearing minerals (Brunetto et al., 2006; Sasaki et al., 2001; Yang et al., 2017; P. Zhang et al., 2022). The disproportionation reaction of Fe<sup>2+</sup> during micrometeoritic impacts has recently been argued to be another possible origin of npFe<sup>0</sup> (Z. Guo, Li, Li, Wen, Tai, et al., 2022; Li, Guo, et al., 2022; Xian et al., 2023). Fe metal inside impact beads may also be generated through the reduction of FeO by oxygen diffusion driven by redox gradients (Pang et al., 2024). A recent study has demonstrated the distinct contributions of solar wind irradiation and meteorite impacts to the production of npFe<sup>0</sup> particles with varying sizes (Shen et al., 2024). Meanwhile, simulation experiments have revealed the complexity of the formation of npFe<sup>0</sup> (Shusterman et al., 2020). These all suggested the complex mechanisms responsible for the formation of npFe<sup>0</sup> inside the agglutinate glass. Newly returned lunar and asteroid samples (such as Hayabusa 1 and 2, Lauretta et al. (2017)) provide new opportunities to study the space weathering recorded by nanoparticles.

In this study, we have described for the first time, np-metals with tails and associated dendritic growths that represent nanoscale products of impact processes within agglutinate melt glass in the Chang'e-5 returned lunar regolith. Dendritic structures, characterized by their tree-like branching patterns, have been observed in various geological contexts on the Moon, Earth and other planets (Arndt & Von Engelhardt, 1987; Kretz, 2003). A recent study has documented a nanoscale intergrowth structure resembling a mushroom, composed of chromite, troilite, and Fe associated with olivine grains in the lunar regolith collected by Chang'e-5 (Xi et al., 2024). This structure has been shown to result from impact-induced non-equilibrium growth processes. We discussed the possible scenarios for producing such nanoscale products. We also interpreted the tadpole-shape nanoparticles provide a new example of viscous fingering and chemical gardens in impact melts. Chemical gardens serve as a remarkable demonstration of self-organizing systems in chemistry, exemplifying the formation of intricate structures through non-equilibrium processes (Barge et al., 2015). Non-equilibrium crystallization and the distinctive dendritic morphology occurring during impact events may represent a prevalent mechanism in the formation of lunar regolith.

## 2. Materials and Methods

Chang'e-5 scooped samples CE5C0400 (200 mg), allocated by the China National Space Administration, which were used in this study. The CE-5 soil is a type of matured lunar soil, in which 95% of particles have sizes between 1.40 and 9.35 μm (Li, Hu, et al., 2022).

The glass beads (larger than 100 μm impact glasses) were picked under a binocular microscope and then transferred to a conductive double-sided sticky carbon tape and coated in carbon to prevent charging. Then, petrographic observations were carried out under a scanning electron microscope (SEM, Helios 5 CX, Thermo Fisher, USA) operating at an accelerating voltage of 25 kV. Experiments were conducted in the State Key Laboratory of Geological Processes and Mineral Resources, and the State Key Laboratory of Metastable

Materials Science and Technology, Yanshan University, China. The surface morphology of the sample was characterized in secondary electron imaging. The qualitative element distribution was measured with an X-ray energy dispersive spectrometer (EDS, XFlash 6/60, Bruker) equipped on the Helios SEM. After these measurements, two glass beads were selected for focused ion beam (FIB) nanofabrication. Thin lamellar specimens with a thickness of approximately 150 nm were prepared using Gallium with an accelerating voltage of 25 kV, and finally thinned to approximately 80 nm using a 50 pA beam at an accelerating voltage of 2 kV. Before being loaded into a transmission electron microscope (TEM), the surficial damaged layer of the specimens was removed with low-energy Ar ion milling (NanoMill, Model 1040, Fischione), and was cleaned with H<sub>2</sub>/O<sub>2</sub> plasma (Plasma Cleaner 695, Gatan) for 40 s to remove possible carbon contamination. In one lamella, remarkable np-metal with tails was found under TEM imaging.

The FIB lamellae specimens were then examined under a spherical-aberration-corrected scanning transmission electron microscope (STEM, Themis Z, Thermo Fisher) with a monochromator, and operating at an accelerating voltage of 300 kV. Bright-field (BF), annular dark field image (ADF) and high angle annular dark field image (HAADF) images were obtained by combining 20 frames from the acquired series with drift correction (DCFI in Velox software, Thermo Fisher). The collecting angle of HAADF was set at 65–200 mrad to eliminate the effects of coherent scattering. The structural analysis of npFe<sup>0</sup> and ilmenite crystals was conducted by comparing the corresponding Fast Fourier Transforms (FFT) of high-resolution HAADF-STEM images with simulated electron diffraction patterns. The EDS maps were obtained by a built-in X-ray energy dispersive spectrometer (SuperX) on Themis Z. The statistical errors were determined from analyzing of over twenty single-point data.

### 3. Results

We studied numerous impact melt glass spherules in our allocated samples and found they all have nanoscale metal particles with various textures similar to those reported by Long et al. (2022) and Yan et al. (2022). Observations show occurrences of unique tadpole-shaped nanophase metal particles in an agglutinate within the sample CE5C0400. The agglutinate consists of a spherical impact glass about 300 μm in diameter that was attached to a shattered lithic fragment composed of olivine, pyroxene, and plagioclase (Figure 1a). On the surface, the melt glass is decorated by several adhesions such as silicates, Fe metal, Fe sulfides, and splash silicate melt deposits that included circular, pancake-shaped, bead-like, and oblong features (Supplementary Figs. S1, S2 in Supporting Information S1). These surface deposits are mostly ~1–5 μm thick, but can be up to 20 μm in some locations. Similar surface adhesives were observed on the CE-5 samples (Yan et al., 2022, e.g.) akin to observations of Apollo lunar soils (Figure S2d in Supporting Information S1) (Ma & Liu, 2019; Wentworth et al., 1999).

To investigate the interior composition and texture at the adhering junction between the glass spherule and lithic fragments, a series of FIB lamellae were prepared. STEM images revealed numerous nanoparticles within the glass component, particularly near the boundary between the olivine grain and the glass. In an area of 9 μm<sup>2</sup> shown in Figure 1b, more than 50 nanoparticles were discovered. Remarkably, most of these nanoparticles have tails (Figures 1b, 2, and 3) that are ~400–500 nm long and ~30–80 nm wide, making them tadpole-shaped. These tails show straight or curved orientations (Figure 1).

Spherical heads of the tadpole-shaped np-metals are mostly (~80%) about 20–110 nm in diameters, and the largest one has a diameter of ~190 nm (Figures 2a, 2b and 3). As shown by the HAADF-STEM images and EDS maps, the composition of the spherical heads varies from Fe, Fe-Ni to Fe-Ni-S (Figure 3, Figure S3 in Supporting Information S1). Of the 15 particles analyzed 3 are Fe-rich with a body-centered cubic (BCC) structure with very low Ni (Fe = 9.6%, and Ni = 0.4%, cell parameter = 0.208 nm). The others are Ni-rich with a face-centered cubic (FCC) structure and a Ni/(Fe + Ni) atomic ratio range from 0.31 to 0.41 (cell parameter = 0.190 nm, Figure 3, Table S2 in Supporting Information S1). The largest tadpole-shaped nanoparticle head is composed of Fe-Ni metal and its “neck” has two discernible individual portions (Figure 2). The inner portion and the outer portions are composed of FeS and ilmenite (FeTiO<sub>3</sub>), respectively, and extend to form a tail about 300 nm long (Figures 2 and 3). Some Fe metal heads were irregularly, or subrounded, while some Fe metals were euhedral (Figures 1 and 4). The Ni-rich metals (FCC structure) were about 20–50 nm, and both the irregularly and euhedral shapes had been found (Figure 4; Figure S5 in Supporting Information S1). The sizes of these Fe-Ni-S nanoparticles were consistent with the size of large particles LnpFe<sup>0</sup> reported in Shen et al. (2024). The metals were always associated with FeS, and the two together formed nearly spherical shapes (Figure 4). They were produced

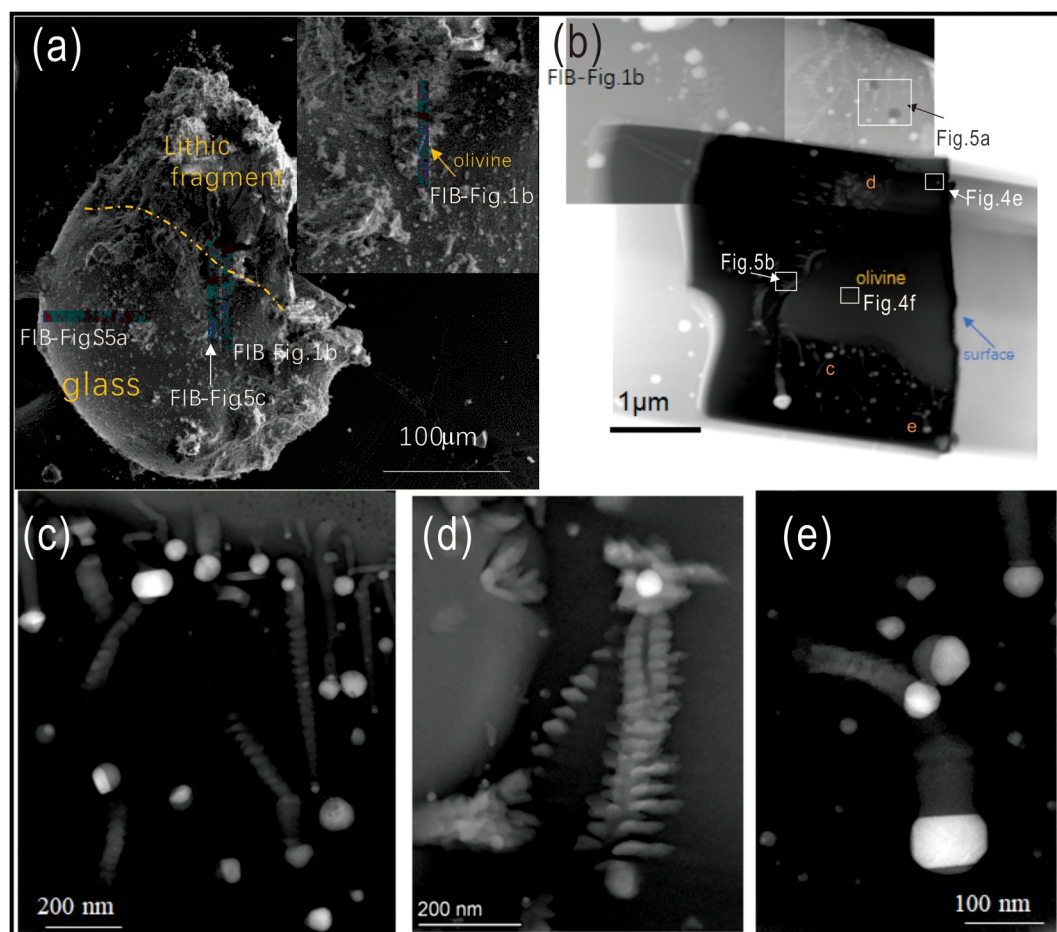


**Figure 1.** The studied agglutinate containing nanoparticles with tails. (a) An overall view of secondary electron (SE) image for the agglutinate. The glass is welded to an olivine grain. The green stripes are the locations for FIB sectioning. (b) Combined HAADF-STEM image of the lamella cut from the glass bead. The contrast difference in different parts of the mosaic is due to different imaging conditions. (c–e) enlarged STEM images show np-metals (white to light gray) and their tails (darker gray).

as globular or irregular inclusions in the impact glass, ranging from pure nano-metal to irregular intergrowths of metal with varying proportions of FeS. Besides, there were cracks and voids around these nano-metals (Figures 4a and 4b).

All tails are composed of ilmenite crystals (Figures 1b, 3, and 5). A second ilmenite-rich area is located nearby and shown in Figure 1b, but deeper in the interior of the melt glass, which also contains unusually well-developed dendritic ilmenite crystals (Figure 5c). All the associated tadpole-shaped nanoparticles occur in the glass spherule adjacent to olivine (Figure 1b). This olivine is irregularly shaped and has an intermediate composition ( $Fo = 48$ , Table S3 in Supporting Information S1), similar to olivine from other Chang'e-5 basalts (He et al., 2022; Tian et al., 2021). X-ray mapping shows that the olivine is compositionally homogenous (Figure S4 in Supporting Information S1). In addition, solar energetic particle tracks occur as crisscrossing straight lines in the olivine grain, closely similar to those observed in Apollo samples (Keller et al., 2021) (Figure S4h in Supporting Information S1).

It should be noted that not all the embedded nanoparticles have visible tails. Some particles without tails may be caused by the viewing angle. Indeed, the FIB lamella may not cut through the tails of some tadpole-shaped nanoparticles so it is likely some tails are invisible. Alternatively, portions of the glass spherules contain abundant nanoparticles that are uniformly absent of tails (Figure S5 in Supporting Information S1). The tail-free nanoparticles are embedded in the same melt glass at a depth of about 1 μm. As shown in Figures S5 and S6 in

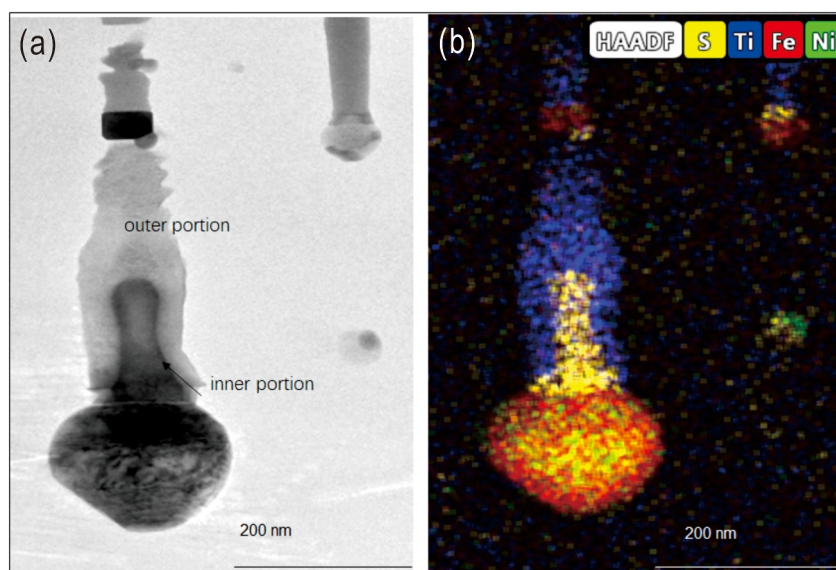


**Figure 2.** High angle annular dark-field (HAADF)-STEM image and EDS map of tadpole-shaped nanoparticles within impact melt glass of an agglutinate from Chang'e-5 lunar soil. (a) BF-STEM image of one of the largest particles and its tail. (b) EDS map of the same region as Figure 1d. 1 It shows the tadpole-shaped head is composed of Fe-Ni-S; its neck is rich in FeS, and the tail is composed of Ti-Fe-O (ilmenite; Figure 3, Table S1 in Supporting Information S1).

Supporting Information S1, these nanoparticles have diameters of 10–75 nm, and are mostly smaller than 50 nm in diameter. Their compositions are also dominated by Fe and some have S (Figure S5 in Supporting Information S1).

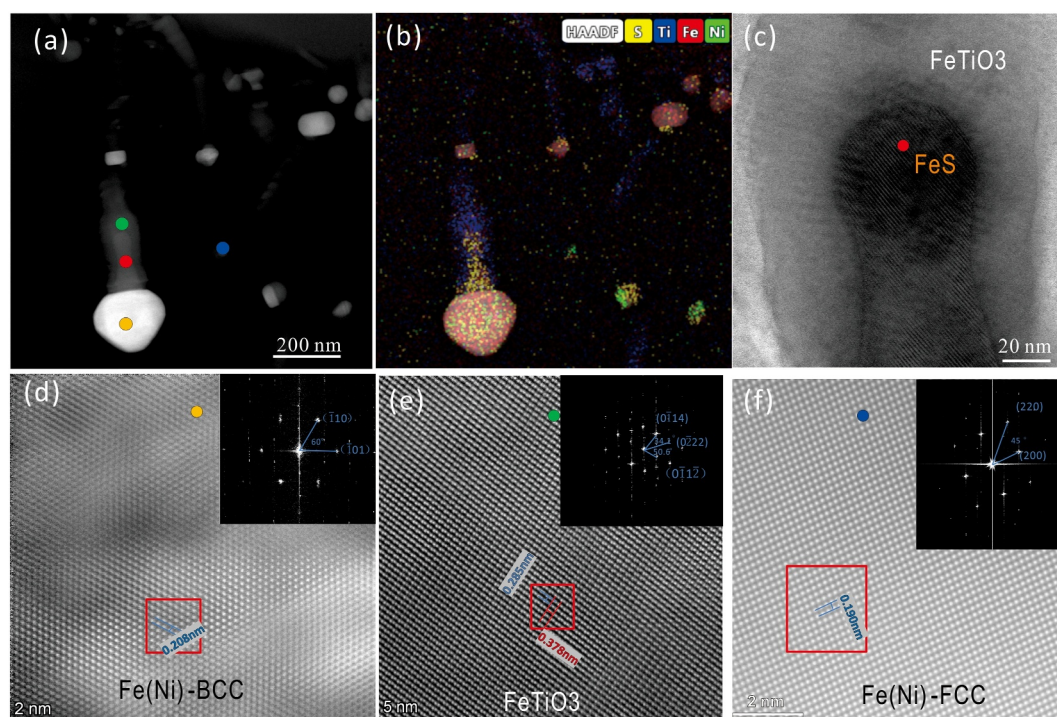


**Figure 3.** Structure and composition of nanoparticles and their tails. (a) Low magnification HAADF-STEM image from part of Figure 1a. (b) The corresponding EDS mapping shows the distribution of Fe, Ni, S, Ti. (c) High-resolution BF-STEM image of the crystallized Fe-S embedded in Ti-Fe-O. (d–f) High-resolution HAADF-STEM images for BCC Fe nanoparticle (head), Ti-Fe-O (tail) and FCC Fe(Ni) structured nanoparticle in a smaller size.

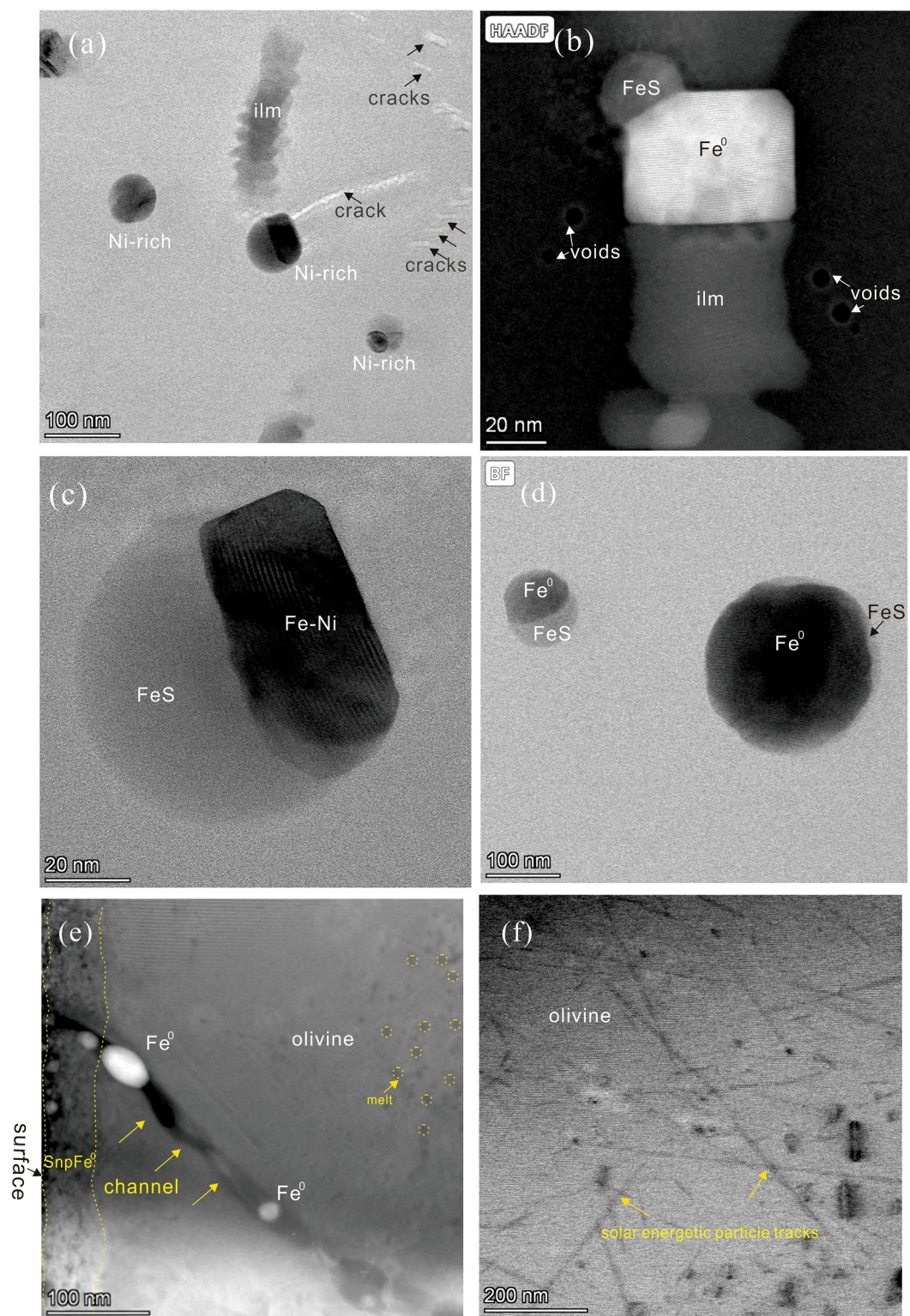


**Figure 4.** High angle annular dark-field (HAADF)-STEM images of Fe metals and Ni-rich metals and olivine. (a–d) STEM images of Fe and Ni-rich metals. (e–f), amplified HAADF images of the olivine. e, the image shows a channel within the olivine. The olivine has a densely distributed SnpFe<sup>0</sup> (small nanoparticles) rim with the thickness of 70 nm, as indicated by the two yellow lines. Within the olivine, it contains some amorphous inclusions which indicate that it had undergone some degree of partial melting. (f), the image shows the presence of solar energetic particle tracks within the olivine. Ilm, ilmenite, Ni-rich, Ni-rich metal.

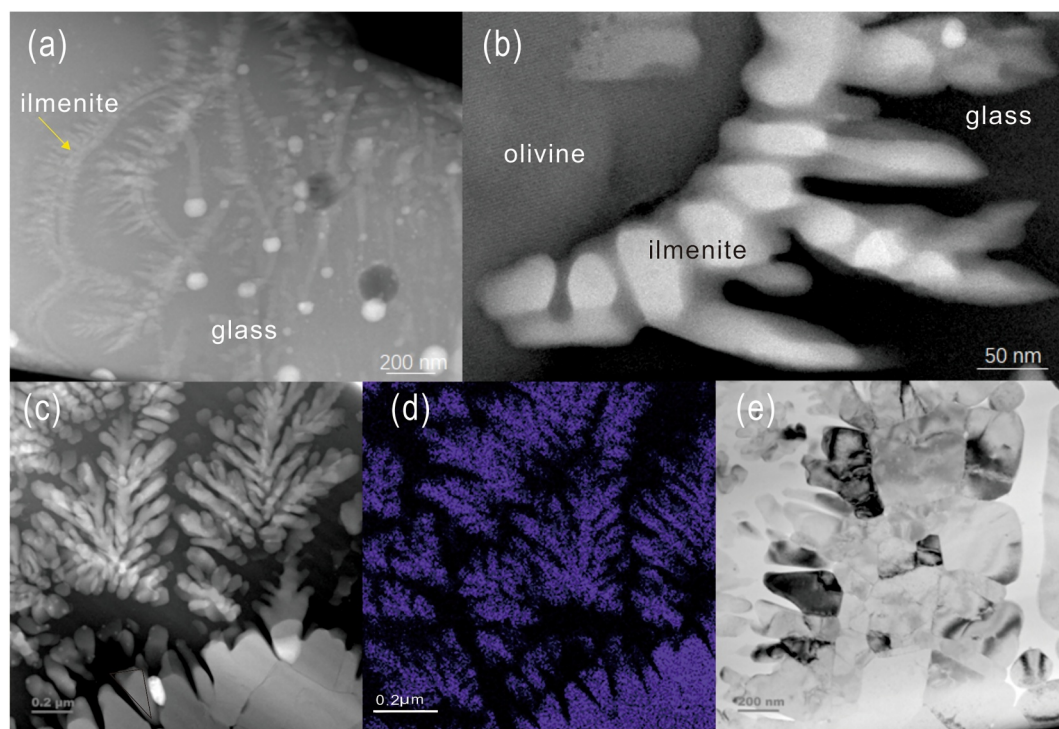


**Figure 5.** Ilmenite tails of tadpole-shaped nanoparticles and associated dendrite and polycrystalline textures within the melt glass. (a) HAADF-STEM image of Fe-Ni nanoparticles with ilmenite tails. (b) Ilmenite dendrites at the boundary between olivine and melt glass. (c) HAADF-STEM image of dendritic ilmenite forming arborescent structures in melt glass. (d) STEM-EDS map of Ti in dendritic ilmenite. (e) BF image of polycrystalline texture of ilmenite dendrites at the bottom of the ilmenite in Figure 5c.

## 4. Discussion

### 4.1. Formation of the Tadpole-Shaped np-Metals

The tadpole-shaped np-metals described above are not reported in previous collections of lunar samples or lunar meteorites. At least two plausible mechanisms might be feasible to explain their formation according to their nanopetrographic context and occurrence on the lunar surface: (a) The crystals of Fe-Ni metal, FeS, and ilmenite are crystallized and grown from the host melt, or (ba) the particles (together with their fine structures) are injected grains into the melt from the exterior of the glass.

Crystallization and growth of small-sized minerals from fast cooling melts are common in nature and laboratory simulation. It has been tested that olivine can decompose to produce nanoparticles such as nanophase Fe (Z. Guo, Li, Li, Wen, Tai, et al., 2022) or wüstite FeO (J.-G. Guo et al., 2022) during space weathering by thermal decomposition. Previous work by Z. Guo, Li, Li, Wen, Tai, et al. (2022) documents the decomposition of olivine in Chang'e-5 soil by meteorite bombardment, and associated layers of Fe nanoparticles. However, the distribution of nanoparticles is radically different than the observations in this study: instead of being aligned along the grain/glass boundary, the nanoparticles are either aligned along the upper surface of the olivine grain or they are notably within the impact melt glass. It is possible that the Chang'e 5 olivine, with 23–123 ppm Ni (He et al., 2022; Su et al., 2023), was exposed to high-temperature during an impact event and be partially melted locally, thereby liberating Fe, Ni into the melt as a reduction reaction. However, the low Ni content in the Chang'e 5 olivine imply that the part of the Ni comes from troilite rather than from the decomposition of olivine. These nanoparticles with relative large size and do not consist solely of Fe but often include S, Ni, and other elements, indicating its non-evaporative olivine decomposition origin (Li et al., 2024).

Another possibility for their formation involves a hypothesized impact vapor plume, which is caused by mutual collisions between glass spherules and other particles during flight (Johnson & Melosh, 2012; Yan et al., 2022). Based on the results of microstructural analyses of CE-5 lunar melt glass, there are many features that possibly

record mutual colliding particles within the impact plume, such as low-velocity induced clustered secondary microcraters and hemispherical iron-rich mounds mainly composed of Fe, with minor Ni, P and S (Yan et al., 2022). During the mutual colliding process, some of Fe-rich mounds can extend into the glass or possibly get injected into the glass. These Fe-rich mounds have relatively large sizes compared to Fe-Ni-S nanoparticles, and they can reach microscopic scales (Yan et al., 2022). However, this model has some weakness. It requires restricted condition for particle implantation.

Some S- and P- bearing Fe nanoparticles around the extremity of impact glass have been argued to from original tiny troilite and schreibersite produced by shock-induced dissemination (Shen et al., 2024). Impacts would probably mix some Fe-Ni-S fractions produced by shock-induced dissemination observed in this study. On the other hand, Fe-rich nanoparticles (composed of  $\alpha$ -Fe and troilite) was considered to form by liquid immiscibility during cooling of impact melt (Yan et al., 2024). Pang et al. (2024) have proposed a new mechanism that Fe nanoparticles are formed due to oxygen diffusion driven by redox potential gradients, which shows concentration gradients of FeO and K<sub>2</sub>O for the impact glasses. However, the nanoparticles are not all  $\alpha$ -Fe and some of them is Ni-rich nanoparticles in this study (Figure 3). Meanwhile, the distributions of Fe-Ni nanoparticles were near the olivine and impact glass boundary (Figure 1) and no obvious Fe compositional gradients had been observed (Figure S6 in Supporting Information S1). Fe-Ni nanoparticles are formed by liquid immiscibility of impact melt, however, cannot be ruled out. Sulfide melt would be immiscible within a silicate melt, and would have a high partition coefficient with Fe and Ni relative to the silicate melt (Hamann et al., 2018). Sulfide plumes of Fe and Ni nanoparticles then separate from the silicate melt and diffuse through the melt forming the nanoparticle necks. Meanwhile, the Desulfurization of FeS resulted in the nucleation of nanophase iron-nickel metal (Li et al., 2024).

Part of the Fe-Ni nanoparticles are euhedral (Figures 1 and 4) which may imply that they may crystallized during cooling of Fe-Ni melt. The melting temperature for the ilmenite is around 1,650°C and Fe- Ni metal is close to 1,500°C. In the scenario where Fe-Ni-S particles were mixed from outside, the Fe-Ni metal nanoparticles are expected to have melted.

#### 4.2. Formation of the Ti-Fe-O Tails

The dendritic ilmenite crystals shown in Figure 5 are similar to the devitrification structure found in lunar melt inclusions (Hauri et al., 2017; Ni et al., 2017) and the Apollo 17 orange glass (Haggerty, 1974). However, heterogeneous nucleation of glass is initiated at unidentified sites on the surface of glass spheres and proceeds toward the interior of the sphere as a distinctly arcuate and cone-shaped zone (Haggerty, 1974). Devitrification structures can occur as relict crystals in lunar melt inclusions that occur as a fine mixture of olivine and ilmenite growth from walls toward the interior of the cone-shaped zone or across the entire inclusion (Hauri et al., 2017; Ni et al., 2017).

The tails of ilmenite in the studied FIB lamellae occur in linear or curved arrangements and they closely follow the Fe-Ni metal composition. However, in 3D, these tails could have fan-like or curvilinear shapes. Hence, the tails could be quenched textures, such that they could represent the beginning stages of devitrified ilmenites, emanating from the Fe-Ni metal, in turn possibly serving as nucleation sites for dendritic growth. The impact melt is saturated with ilmenite and contains more than 9 wt.% TiO<sub>2</sub> (Table S3 in Supporting Information S1), and therefore has a suitable composition to form dendritic ilmenite. However, recent studies show that the basalts near Chang'e-5 are Ti-poor, which rather supports an exogenous or distal source for this ilmenite-rich impact glass (D. Zhang et al., 2022). Ultimately, the ilmenite likely nucleates as a result of the passage of npFe<sup>0</sup> through the melt, which may contribute to a change in oxidation state of the melt to allow for nucleation to occur, and then grow through rapid quenching. The images of the dendrites show a "seam" through the middle of them (Figure 5a), which confirms where the common nucleation point for these symmetrical crystals is located.

Recently, a mushroom shaped intergrowth structure of chromite, troilite and np Fe attached to olivine has been reported in the Chang'e-5 lunar soil (Xi et al., 2024). The structure is similar to the tadpole-shaped nanoparticles study here. The shape is similar and both occurred in the interface of olivine and impact glass. The mushroom intergrowth was proved formed though impact-induced nonequilibrium growth and chromite was supported to originate from olivine. The impact-induced nonequilibrium growth was a common mode occurred on the heterogeneous interfaces which also take place here in this study. However, the tails were ilmenite not chromite.

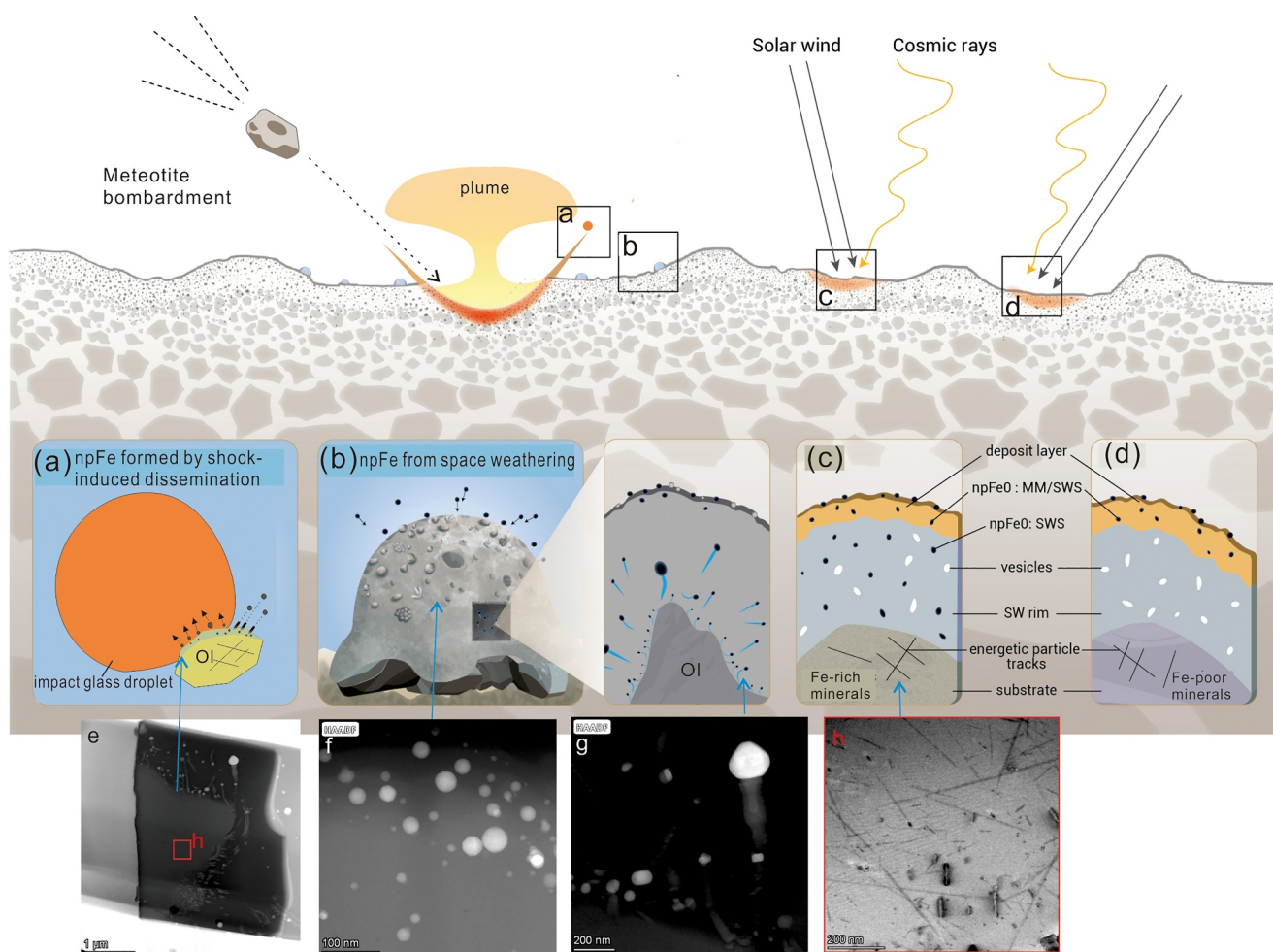


**Figure 6.** Space weathering and possible formation mechanisms of nanoparticle metals within lunar agglutinates and minerals. (a) Fusion of impact melt onto an olivine grain. Fe-Ni nanoparticles produced by shock-induced dissemination and the shock also allowed the Fe nanoparticle migration and caused nucleation of Ti oxides. (b) The nanoparticles formed from space weathering after the impact melt solidified and then the host melt glass coated with later deposition of npFe<sup>0</sup> and np-metals sulfides and silicates on the surface by later micrometeorite impact process. (c) The space weathering effect on Fe-bearing minerals (modified after Gu et al. (2022)). (d) The space weathering effect on Fe-free minerals (modified after Gu et al. (2022)). MM-micrometeorite, SWS-solar wind sputtering, SW-solar wind.

Meanwhile, ilmenite tails in our samples originated from impact glass, which is rich in Ti and different from the chromite mushroom.

Some tadpole-shaped nanoparticles had been transported away from the olivine, which also implying during the impact system, the nanoparticles derived from olivine or impact glass, would move and transported away from the olivine surface. The process also records the movement and migration of Fe-Ni nanoparticles and the migration of the Fe-Ni particles may locally change the oxidation conditions of the impact melt.

### 4.3. Implication for the Origin of np-Metals in Lunar Soil

Two formation pathways can be involved for the formation of the Fe-Ni-S nanoparticles. One is the production of Fe-Ni metal nanoparticles from by shock-induced dissemination (Shen et al., 2024), accompanied by Fe-Ni particle migration, which causes nucleation of Ti oxides (Figure 6a). The other is that the tail-free nanoparticles (Figure 6b) form from another pathway, and possibly after the impact glass solidified.

There are similar types of Fe nanoparticles forming under space weathering conditions (Taylor et al., 2001; Z. Guo, Li, Li, Wen, Tai, et al., 2022; Gu et al., 2022). What is significantly different in this study is the geometry and nanotexture of the system. Many previous studies also report npFe<sup>0</sup> formed by solar wind sputtering on mineral grains (Keller & McKay, 1997; Noguchi et al., 2011; Thompson et al., 2022). The composition of targeted

minerals is an important factor in the formation of  $\text{npFe}^0$  in mineral rims. The space weathering features of different mineral grains in Chang'e-5 lunar soil are recent topics of studies (Gu et al., 2022). They found that all minerals, except for iron sulfide, have a vapor deposited layer induced by micrometeorite impacts or solar wind irradiation, and the thickness of this layer is different depending on different host minerals. Below this vapor deposited layer is the solar wind irradiation rim, where  $\text{npFe}^0$  particles can be only found in Fe-bearing minerals (Gu et al., 2022). In this rim,  $\text{npFe}^0$  particles are spherical in the pyroxenes, elongated in ilmenite. The lowermost rim is where solar energetic particle tracks penetrate both Fe-bearing and Fe-free minerals. With continued space weathering, an uppermost thin  $\text{npFe}^0$ -bearing layer can form on Fe-bearing minerals by both vapor deposition followed by later micrometeorite bombardment and solar wind sputtering. In contrast, Ca-plagioclase grains with a  $\text{npFe}^0$  bearing vapor deposit layer may suggest an exotic origin such as nearby olivine crystal (Cymes et al., 2021). The formation mechanisms of nanoparticle metal origins are summarized in Figure 6.

#### 4.4. Implication of High-Temperature Chemical Gardens in Lunar Soil

In this work, tadpole-shape nanoparticles are suggested to be formed from the fusion of impact melt to an olivine grain, which requires a high temperature physical process. As these tadpole-shape nanoparticles are closely associated with dendritic ilmenite, processes linked to high temperature diffusion-limited aggregation (DLA) and “viscous fingering” (Homsy, 1987) might have been involved. Early studies of dendritic patterns in natural objects have been qualitatively described by DLA growth mechanisms, which are associated with viscous fingering, known to produce arborescent or finger-like growths (García-Ruiz et al., 1994; Mandelbrot, 1989). These works have shown examples of arborescent patterns formed when a less dense, less viscous fluid penetrates a more dense, more viscous, and immiscible fluid. This produces fractal patterns (i.e., a self-similar pattern with various size dimension scales) using a large Hele-Shaw cell tipped into vertical position or with interfacial boundaries, thereby forming fingering growths with morphologies akin to those of the lunar tadpole-shape nanoparticles. In the context of lunar impact melt, this phenomenon can occur when a viscous solution displaces a more viscous one. In other words, during impact process, Fe-Ni bearing part had mixed and migrated in melt when fusion to the olivine. The less viscous solution containing sulfur volatiles (with highly variable Fe, Ni) diffuses in the “tadpole head”, whereas the more viscous solution remains as the melt glass.

The tadpole-like structures are also similar to probable VLS (vapor-liquid-solid)-type growth of mixture of Fe and S have been reported on the lunar surface (Carter, 1973). However, the situation is different and the tadpole-like structures occur only in the melt. Growth of VLS-type mixtures with compositions inferred from the new observations can also explain the morphology of tadpole-like structures with a metal droplet at the head and an elongated tail showing its diffusion direction.

However, these explanations could also be compatible with each other and ultimately, the dendritic ilmenite habits can be used to interpret the formation of tadpole-like structures such as in chemical garden experiments. Chemical gardens are abiotic, self-organizing, and out-of-equilibrium processes that create complex structures (Barge et al., 2015), and their discovery in melt glasses from lunar soils shows the existence of such processes also occurring at lunar impact melts. Therefore, the tadpole-shape Fe-Ni nanoparticles and associated ilmenite dendrites point to the influence of viscous fingering, DLA, and VLS during the formation of high-temperature chemical gardens in lunar impact melt. This finding suggests that non-equilibrium crystallization occurs during the impact process. It is conceivable that non-equilibrium crystallization and chemical gardens may be common phenomena in lunar soils. Previously, research on space weathering primarily focused on physical weathering processes such as crushing, melting, cementation, and mixing. However, this study reveals that chemical processes are equally important, particularly at the particle scale (ranging from nanometers to millimeters). During high-temperature melting events caused by impacts, a significant number of chemical reactions can occur.

Thermal decomposition of olivine, disproportionation reactions (Z. Guo, Li, Li, Wen, Tai, et al., 2022; Li, Guo, et al., 2022), and the formation of magnetite (Z. Guo, Li, Li, Wen, Wu, et al., 2022) can also be categorized as chemical processes. Non-equilibrium crystallization, crystal growth, and other dynamic processes are highly active and contribute significantly to the chemical changes occurring on the lunar surface. Given the frequent impacts and complex environmental conditions on the Moon, these mechanisms are likely common in lunar regolith and may also be prevalent in the regolith of other planetary bodies. This area warrants further research attention in the future.

Dendritic structures have been previously reported in both terrestrial and extraterrestrial samples. There are also accounts of diagenetic dendrites on Mars (Nachon et al., 2017). Additionally, dendritic magnetite associated with ilmenite (500–540  $\mu\text{m}$  across) occurs in gabbro dikes has been documented in Otter Lake, Quebec (Kretz, 2003). Arndt and Englehardt (Arndt & Von Engelhardt, 1987) discovered ilmenite “dendritic spikes” on olivine surfaces in Apollo 17 orange glass beads. In this study, the dendritic ilmenites were formed during high-temperature impact processes, resembling chemical gardens. Further detailed experiments are needed to explore the geochemical and thermodynamic conditions necessary for the formation of chemical gardens. A better understanding of these abiotic processes augments the repertoire of physical and geochemical condition from which abiotic biomorphs can form, which is important for astrobiology and understanding why chemical gardens exist.

## 5. Conclusions

In this study, we discovered tadpole-shaped Fe-Ni-(S) nanoparticles with distinctive ilmenite tails within the glass grain, situated at the boundary between olivine and impact glass. The head of each Fe-Ni nanoparticle, composed of Fe-Ni metal, appeared in both euhedral and anhedral forms, exhibiting both body-centered cubic (BCC) and face-centered cubic (FCC) structures. The formation of these nanoparticle heads, each containing S-bearing part approximately tens to hundreds of nanometers, is hypothesized to be a result of impact-induced dissemination. However, we cannot discount the possibility that the formation mechanisms may also be contributed to liquid immiscibility within the impact glass. The tails of these nanoparticles are comprised of devitrified ilmenite, which nucleated as the Fe-Ni nanoparticles traversed the melt. The formation of these nanoparticles is attributed to an impact-induced nonequilibrium growth process, capturing the dynamic movement and migration of the Fe-Ni nanoparticles through the melt. The tadpole-shaped nanoparticles exemplify a novel instance of viscous fingering within impact melts, while the associated ilmenite dendrites suggest the emergence of high-temperature chemical gardens in lunar impact melts. These chemical gardens offer valuable insights into the complex interactions between the space environment and the surfaces of other airless celestial bodies.

## Data Availability Statement

The data reported in this work can be found in the Supporting Information S1 and Mendeley Data under (He, 2023).

## Acknowledgments

We appreciate the China National Space Administration (CNSA) for organizing and implementing the CE-5 mission and providing access to the CE-5 sample CESC0400. Many thanks also go to the colleagues in the State Key Laboratory of Geological Processes and Mineral Resources, China University of Geosciences, Wuhan for providing technical support. This research is funded by the National Key R & D Program of China (2023YFB3711300, 2020YFE0202100), the National Natural Science Foundation of China (42241111), and the Science and Technology Development Fund of Macau (Grant 0052/2024/RIA1). The authors are grateful to Shaofan Che, Te Jiang and Clive R. Neal for discussion.

## References

- Arndt, J., & Von Engelhardt, W. (1987). Formation of Apollo 17 orange and black glass beads. *Journal of Geophysical Research*, 92(B4), E372–E376. <https://doi.org/10.1029/jb092ib04p0e372>
- Barge, L. M., Cardoso, S. S., Cartwright, J. H., Cooper, G. J., Cronin, L., De Wit, A., et al. (2015). From chemical gardens to chemobionics. *Chemical Reviews*, 115(16), 8652–8703. <https://doi.org/10.1021/acs.chemrev.5b00014>
- Basu, A. (2005). Nanophase Fe 0 in lunar soils. *Journal of Earth System Science*, 114(3), 375–380. <https://doi.org/10.1007/bf02702956>
- Britt, D., & Pieters, C. (1994). Darkening in black and gas-rich ordinary chondrites: The spectral effects of opaque morphology and distribution. *Geochimica et Cosmochimica Acta*, 58(18), 3905–3919. [https://doi.org/10.1016/0016-7037\(94\)90370-0](https://doi.org/10.1016/0016-7037(94)90370-0)
- Brunetto, R., Romano, F., Blanco, A., Fonti, S., Martino, M., Orofino, V., & Verrienti, C. (2006). Space weathering of silicates simulated by nanosecond pulse UV excimer laser. *Icarus*, 180(2), 546–554. <https://doi.org/10.1016/j.icarus.2005.10.016>
- Carter, J. L. (1973). VLS (vapor-liquid-solid): Newly discovered growth mechanism on the lunar surface? *Science*, 181(4102), 841–842. <https://doi.org/10.1126/science.181.4102.841>
- Cymes, B., Burgess, K., Stroud, R., Team, A. S., et al. (2021). Nanoscale insights into Apollo 17 regolith samples from stations 2 and 6: Exposure history, mineral phase composition, and space weathering. In *52nd lunar and planetary science conference* (p. 1152).
- García-Ruiz, J. M., Otálora, F., Sanchez-Navas, A., & Higes-Rolando, F. J. (1994). The formation of manganese dendrites as the mineral record of flow structures. In *Fractals and dynamic systems in geoscience* (pp. 307–318).
- Gopon, P., Spicuzza, M. J., Kelly, T. F., Reinhard, D., Prosa, T. J., & Fournelle, J. (2017). Ultra-reduced phases in Apollo 16 regolith: Combined field emission electron probe microanalysis and atom probe tomography of submicron Fe-Si grains in Apollo 16 sample 61500. *Meteoritics & Planetary Sciences*, 52(9), 1941–1962. <https://doi.org/10.1111/maps.12899>
- Gu, L., Chen, Y., Xu, Y., Tang, X., Lin, Y., Noguchi, T., & Li, J. (2022). Space weathering of the Chang’e-5 lunar sample from a mid-high latitude occurs in gabbro dikes has been documented region on the moon. *Geophysical Research Letters*, 49(7), e2022GL097875. <https://doi.org/10.1029/2022gl097875>
- Gu, L., Zhang, B., Hu, S., Noguchi, T., Hidaka, H., & Lin, Y. (2018). The discovery of silicon oxide nanoparticles in space-weathered of Apollo 15 lunar soil grains. *Icarus*, 303, 47–52. <https://doi.org/10.1016/j.icarus.2017.12.028>
- Guo, J.-G., Ying, T., Gao, H., Chen, X., Song, Y., Lin, T., et al. (2022). Surface microstructures of lunar soil returned by Chang’e-5 mission reveal an intermediate stage in space weathering process. *Science Bulletin*, 67(16), 1696–1701. <https://doi.org/10.1016/j.scib.2022.06.019>
- Guo, Z., Li, C., Li, Y., Wen, Y., Tai, K., Li, X., et al. (2022). Nanophase iron particles derived from fayalitic olivine decomposition in Chang’e-5 lunar soil: Implications for thermal effects during impacts. *Geophysical Research Letters*, 49(5), e2021GL097323. <https://doi.org/10.1029/2021gl097323>
- Guo, Z., Li, C., Li, Y., Wen, Y., Wu, Y., Jia, B., et al. (2022). Sub-microscopic magnetite and metallic iron particles formed by eutectic reaction in Chang’e-5 lunar soil. *Nature Communications*, 13(1), 7177. <https://doi.org/10.1038/s41467-022-35009-7>

- Haggerty, S. E. (1974). Apollo 17 orange glass-textural and morphological characteristics of devitrification. In *Lunar science conference, 5th, Houston, Tex., March 18-22, 1974, proceedings* (Vol. 5, pp. 193–205). Pergamon Press, Inc.
- Hamann, C., Fazio, A., Ebert, M., Hecht, L., Wirth, R., Folco, L., et al. (2018). Silicate liquid immiscibility in impact melts. *Meteoritics & Planetary Sciences*, 53(8), 1594–1632. <https://doi.org/10.1111/maps.12907>
- Hapke, B. (2001). Space weathering from mercury to the asteroid belt. *Journal of Geophysical Research*, 106(E5), 10039–10073. <https://doi.org/10.1029/2000je001338>
- Hauri, E. H., Saal, A. E., Nakajima, M., Anand, M., Rutherford, M. J., Van Orman, J. A., & Le Voyer, M. (2017). Origin and evolution of water in the moon's interior. *Annual Review of Earth and Planetary Sciences*, 45(1), 89–111. <https://doi.org/10.1146/annurev-earth-063016-020239>
- He, Q. (2023). Tadpole-shaped nanoparticles in impact melt and implication for the origin of Nano-metals in lunar soil [Dataset]. <https://doi.org/10.17632/2z9bfj5sk6.2>
- He, Q., Li, Y., Baziotis, I., Qian, Y., Xiao, L., Wang, Z., et al. (2022). Detailed petrogenesis of the unsampled Oceanus procellarum: The case of the Chang'e-5 mare basalts. *Icarus*, 383, 115082. <https://doi.org/10.1016/j.icarus.2022.115082>
- Heiken, G. (1975). Petrology of lunar soils. *Reviews of Geophysics*, 13(4), 567–587. <https://doi.org/10.1029/rg013i004p00567>
- Homsy, G. M. (1987). Viscous fingering in porous media. *Annual Review of Fluid Mechanics*, 19(1), 271–311. <https://doi.org/10.1146/annurev.fluid.19.1.271>
- Housley, R. M., Grant, R. W., & Paton, N. (1973). Origin and characteristics of excess Fe metal in lunar glass welded aggregates. In *Proceedings of the lunar science conference* (Vol. 4, p. 2737).
- Johnson, B., & Melosh, H. (2012). Formation of spherules in impact produced vapor plumes. *Icarus*, 217(1), 416–430. <https://doi.org/10.1016/j.icarus.2011.11.020>
- Keller, L. P., Berger, E. L., Zhang, S., & Christoffersen, R. (2021). Solar energetic particle tracks in lunar samples: A transmission electron microscope calibration and implications for lunar space weathering. *Meteoritics & Planetary Sciences*, 56(9), 1685–1707. <https://doi.org/10.1111/maps.13732>
- Keller, L. P., & McKay, D. S. (1993). Discovery of vapor deposits in the lunar regolith. *Science*, 261(5126), 1305–1307. <https://doi.org/10.1126/science.261.5126.1305>
- Keller, L. P., & McKay, D. S. (1997). The nature and origin of rims on lunar soil grains. *Geochimica et Cosmochimica Acta*, 61(11), 2331–2341. [https://doi.org/10.1016/s0016-7037\(97\)00085-9](https://doi.org/10.1016/s0016-7037(97)00085-9)
- Kretz, R. (2003). Dendritic magnetite and ilmenite in 590 Ma grenville dikes near Otter Lake, Quebec, Canada. *The Canadian Mineralogist*, 41(4), 1049–1059. <https://doi.org/10.2113/gscanmin.41.4.1049>
- Lauretta, D., Balram-Knutson, S., Beshore, E., Boynton, W., Drouet d'Aubigny, C., DellaGiustina, D., et al. (2017). Osiris-rex: Sample return from asteroid (101955) bennu. *Space Science Reviews*, 212(1–2), 925–984. <https://doi.org/10.1007/s11214-017-0405-1>
- Li, C., Guo, Z., Li, Y., Tai, K., Wei, K., Li, X., et al. (2022). Impact-driven disproportionation origin of nanophase iron particles in Chang'e-5 lunar soil sample. *Nature Astronomy*, 6(10), 1156–1162. <https://doi.org/10.1038/s41550-022-01763-3>
- Li, C., Hu, H., Yang, M.-F., Pei, Z.-Y., Zhou, Q., Ren, X., et al. (2022). Characteristics of the lunar samples returned by the Chang'e-5 mission. *National Science Review*, 9(2), nwab188. <https://doi.org/10.1093/nsr/nwab188>
- Li, C., Li, Y., Wei, K., Guo, Z., Li, R., Li, X., et al. (2024). Impact-dispersed Fe–Fe1-s core-shell particles in Chang'e-5 lunar soil impact glass. *Geochimica et Cosmochimica Acta*, 379, 134–144. <https://doi.org/10.1016/j.gca.2024.06.038>
- Long, T., Qian, Y., Norman, M. D., Miljkovic, K., Crow, C., Head, J. W., et al. (2022). Constraining the formation and transport of lunar impact glasses using the ages and chemical compositions of Chang'e-5 glass beads. *Science Advances*, 8(39), eabq2542. <https://doi.org/10.1126/sciadv.abq2542>
- Lucey, P. G., & Noble, S. K. (2008). Experimental test of a radiative transfer model of the optical effects of space weathering. *Icarus*, 197(1), 348–353. <https://doi.org/10.1016/j.icarus.2008.05.008>
- Ma, C., & Liu, Y. (2019). Discovery of a zinc-rich mineral on the surface of lunar orange pyroclastic beads. *American Mineralogist*, 104(3), 447–452. <https://doi.org/10.2138/am-2019-6896>
- Mandelbrot, B. B. (1989). Fractal geometry: What is it, and what does it do? *Proceedings of the Royal Society of London. A. Mathematical and Physical Sciences* (Vol. 423(1864), 3–16). <https://doi.org/10.1515/9781400861040.3>
- Matsumoto, T., Noguchi, T., Tobimatsu, Y., Harries, D., Langenhorst, F., Miyake, A., & Hidaka, H. (2021). Space weathering of iron sulfides in the lunar surface environment. *Geochimica et Cosmochimica Acta*, 299, 69–84. <https://doi.org/10.1016/j.gca.2021.02.013>
- Nachon, M., Mangold, N., Forni, O., Kah, L. C., Cousin, A., Wiens, R. C., et al. (2017). Chemistry of diagenetic features analyzed by chemcam at Pahrump hills, gale crater, mars. *Icarus*, 281, 121–136. <https://doi.org/10.1016/j.icarus.2016.08.026>
- Ni, P., Zhang, Y., & Guan, Y. (2017). Volatile loss during homogenization of lunar melt inclusions. *Earth and Planetary Science Letters*, 478, 214–224. <https://doi.org/10.1016/j.epsl.2017.09.010>
- Noble, S. K., Pieters, C. M., & Keller, L. P. (2007). An experimental approach to understanding the optical effects of space weathering. *Icarus*, 192(2), 629–642. <https://doi.org/10.1016/j.icarus.2007.07.021>
- Noguchi, T., Nakamura, T., Kimura, M., Zolensky, M., Tanaka, M., Hashimoto, T., et al. (2011). Incipient space weathering observed on the surface of itokawa dust particles. *Science*, 333(6046), 1121–1125. <https://doi.org/10.1126/science.1207794>
- Pang, R., Yang, J., Li, R., Liu, S., Li, Q., Zhu, D., et al. (2024). Redox condition changes caused by impacts: Insights from Chang'e-5 lunar glass beads. *Science Bulletin*, 69(10), 1495–1505. <https://doi.org/10.1016/j.scib.2024.03.004>
- Pieters, C. M., & Noble, S. K. (2016). Space weathering on airless bodies. *Journal of Geophysical Research: Planets*, 121(10), 1865–1884. <https://doi.org/10.1002/2016je005128>
- Pieters, C. M., Taylor, L. A., Noble, S. K., Keller, L. P., Hapke, B., Morris, R. V., et al. (2000). Space weathering on airless bodies: Resolving a mystery with lunar samples. *Meteoritics & Planetary Sciences*, 35(5), 1101–1107. <https://doi.org/10.1111/j.1945-5100.2000.tb01496.x>
- Sasaki, S., Nakamura, K., Hamabe, Y., Kurahashi, E., & Hiroi, T. (2001). Production of iron nanoparticles by laser irradiation in a simulation of lunar-like space weathering. *Nature*, 410(6828), 555–557. <https://doi.org/10.1038/35069013>
- Shen, L., Zhao, R., Chang, C., Yu, J., Xiao, D., Bai, H., et al. (2024). Separate effects of irradiation and impacts on lunar metallic iron formation observed in Chang'e-5 samples. *Nature Astronomy*, 8, 1–9. <https://doi.org/10.1038/s41550-024-02300-0>
- Shusterman, M., Sharp, T., Robinson, M., Rahman, Z., Keller, L., Dukes, C., et al. (2020). The role of solar wind hydrogen in space weathering: Insights from laboratory-irradiated Northwest Africa 12008. In *Lunar and planetary science conference (lpsc)*.
- Su, B., Zhang, D., Chen, Y., Yang, W., Mao, Q., Li, X.-H., & Wu, F.-Y. (2023). Low Ni and Co olivine in Chang'e-5 basalts reveals the origin of the young volcanism on the moon. *Science Bulletin*, 68(17), 1918–1927. <https://doi.org/10.1016/j.scib.2023.07.020>
- Taylor, L. A., Pieters, C. M., Keller, L. P., Morris, R. V., & McKay, D. S. (2001). Lunar mare soils: Space weathering and the major effects of surface-correlated nanophase Fe. *Journal of Geophysical Research*, 106(E11), 27985–27999. <https://doi.org/10.1029/2000je001402>

- Thompson, M., Barnes, J., Blewett, D., Cahill, J., Denevi, B., Donaldson Hanna, K., et al. (2021). Space weathering across the solar system: Lessons from the moon and outstanding questions. *Bulletin of the American Astronomical Society*, 53(4), 172. <https://doi.org/10.3847/25c2cfeb.0bd09213>
- Thompson, M., Zanetta, P.-M., Zega, T., Noguchi, T., Yurimoto, H., & Nakamura, T. (2022). Evidence for micrometeoroid bombardment on the surface of asteroid Ryugu. *53rd lunar and planetary science conference*, 2678, 2134.
- Tian, H.-C., Wang, H., Chen, Y., Yang, W., Zhou, Q., Zhang, C., et al. (2021). Non-kreep origin for Chang'e-5 basalts in the procellarum creep terrane. *Nature*, 600(7887), 59–63. <https://doi.org/10.1038/s41586-021-04119-5>
- Wang, K., Moynier, F., Podosek, F. A., & Foriel, J. (2012). An iron isotope perspective on the origin of the nanophase metallic iron in lunar regolith. *Earth and Planetary Science Letters*, 337, 17–24. <https://doi.org/10.1016/j.epsl.2012.05.021>
- Wentworth, S. J., Keller, L. P., McKAY, D. S., & Morris, R. V. (1999). Space weathering on the moon: Patina on Apollo 17 samples 75075 and 76015. *Meteoritics & Planetary Sciences*, 34(4), 593–603. <https://doi.org/10.1111/j.1945-5100.1999.tb01366.x>
- Xi, J., Yang, Y., He, H., Xian, H., Li, S., Lin, X., et al. (2024). Mushroom-shaped growth of crystals on the moon. *American Mineralogist*. <https://doi.org/10.2138/am-2023-9214>
- Xian, H., Zhu, J., Yang, Y., Li, S., Lin, X., Xi, J., et al. (2023). Ubiquitous and progressively increasing ferric iron content on the lunar surfaces revealed by the Chang'e-5 sample. *Nature Astronomy*, 7(3), 280–286. <https://doi.org/10.1038/s41550-022-01855-0>
- Yan, P., Xiao, Z., Wu, Y., Pan, Q., & Wu, Y. (2024). Iron-rich grain-decorated depressions on surfaces of lunar impact glasses. *Journal of Geophysical Research: Planets*, 129(4), e2024JE008284. <https://doi.org/10.1029/2024je008284>
- Yan, P., Xiao, Z., Wu, Y., Yang, W., Li, J.-H., Gu, L.-X., et al. (2022). Intricate regolith reworking processes revealed by microstructures on lunar impact glasses. *Journal of Geophysical Research: Planets*, 127(12), e2022JE007260. <https://doi.org/10.1029/2022je007260>
- Yang, Y., Zhang, H., Wang, Z., Yuan, Y., Li, S., Hsu, W., & Liu, C. (2017). Optical spectroscopic characterizations of laser irradiated olivine grains. *Astronomy & Astrophysics*, 597, A50. <https://doi.org/10.1051/0004-6361/201629327>
- Zhang, D., Su, B., Chen, Y., Yang, W., Mao, Q., & Jia, L.-H. (2022). Titanium in olivine reveals low-TI origin of the Chang'e-5 lunar basalts. *Lithos*, 414, 106639. <https://doi.org/10.1016/j.lithos.2022.106639>
- Zhang, P., Tai, K., Li, Y., Zhang, J., Lantz, C., & Hiroi, T. (2022). Diverse space weathering effects on asteroid surfaces as inferred via laser irradiation of meteorites. *Astronomy & Astrophysics*, 659, A78.